

## Meson exchange current contribution to $K^+$ -nucleus scattering

M. F. Jiang and Daniel S. Koltun

*Department of Physics and Astronomy, University of Rochester, Rochester, New York 14627*

(Received 27 July 1992)

We investigate the meson exchange current (MEC) contribution to  $K^+$ -nucleus elastic scattering. Starting with a model of the off-shell  $K\pi$  scattering amplitude and a calculation of the excess pion distribution in finite nuclei, we proceed to derive both real and imaginary forward scattering amplitudes for the MEC contribution. The resulting amplitudes interfere constructively with the optical model amplitudes, and, therefore, lead to an increase in both calculated total and differential cross sections. This increase brings about a better agreement with the data, in particular with regard to the energy dependence of the total cross section. This last feature follows from the fact that the calculated imaginary MEC amplitude has a threshold at incident momentum  $p \sim 400$  MeV/c, which distinguishes our MEC model from recently proposed nucleon "swelling" models. We also examine the sources of uncertainties for our results.

PACS number(s): 25.80.Nv, 24.10.-i, 13.75.Lb

### I. INTRODUCTION

Recent experimental [1–5] and theoretical [6–12] work on  $K^+$ -nucleus scattering has raised some puzzling questions. Since the  $K^+$ -nucleon system exhibits the weakest of the hadron-nucleon interactions at lower energies, with no resonances or bound states, it is expected that microscopic optical potentials should be calculable and reliable. With weaker interactions than the  $\pi$ , nucleon, or antinucleon, multiple-scattering corrections (with their uncertainties) should be considerably less important for the  $K^+$ . In addition, there are no true absorption processes to interfere with multiple scattering. Therefore, one expects the theoretical description of elastic and total  $K^+$ -nucleus cross sections by microscopic optical models to be reasonably accurate.

However, apparent discrepancies between experimental data and optical model calculations have persisted, and are not yet resolved. The original problem was for the elastic differential cross section for  $K^+{}^{12}\text{C}$ , measured at a laboratory momentum of  $p = 800$  MeV/c [2], and analyzed by Siegel, Kaufmann, and Gibbs [6,7]. The calculated cross sections are systematically lower than the data, although for this case there may be sufficient experimental uncertainty to remove the apparent discrepancy. Siegel *et al.* [7] showed that the total cross section  $\sigma_t$ , and in particular the ratio  $R = \sigma_t(K^+A) / (A/2)\sigma_t(K^+d)$ , would be a more sensitive test. A number of measurements of  $R$  now exist for 450 MeV/c  $< p < 1$  GeV/c for  $K^+{}^{12}\text{C}$  [1,3–4], and for several other targets [5]. Again, the values of  $R$  [or  $\sigma_t(K^+A)$ ] calculated from optical theory are smaller than the data, with larger deviations at the higher momenta. Here the experimental uncertainties are small enough to make it probable that the discrepancies are real.

There are unresolved issues in the optical potential calculations. Siegel *et al.* [7] give a range of theoretical uncertainties which still excludes the data for  $R$ . Chen and

Ernst [11] also calculate values of  $R$  10–20% smaller than experiment—but not completely in agreement with Ref. [7]. On the other hand, Berdnikov and Makhov [10] do obtain a good fit to the  $R$  data with an optical potential, but only at the cost of introducing rather different proton and neutron density distributions, which would seem to require a large violation of isospin symmetry for  ${}^{12}\text{C}$ .

As possible explanations of the discrepancies, several novel corrections have been proposed. Siegel *et al.* [7] suggest that the nuclear medium may modify the  $S_{11}$   $K^+$  scattering amplitude by altering the effective nucleon size in the nucleus. They find that an increase of 10–20% in the  $S_{11}$  phase shift would increase the theoretically calculated ratio and lead to an improvement over the deficit. A similar proposal by Brown *et al.* [8] ascribes the modification to the nuclear medium effect on the mass of the vector meson in a boson exchange model for the  $K^+N$  scattering. They find that a density-dependent decrease in the vector meson masses leads to an increase in the repulsion of the kaon and, hence, an increase in the cross section. Both these proposals are related to the so-called nucleon *swelling* concept in the nuclear environment, and the resulting improvements over the discrepancy are very similar, giving more or less a constant increase of  $R$  over the whole momentum range considered (see also Ref. [9]).

In this paper we propose a meson exchange current (MEC) model to account for the contribution to  $K^+$ -nucleus cross sections of  $K^+$  scattering by virtual mesons exchanged within the nuclear target [see Fig. 1(a)]. We expect the dominant exchange to be that of  $\pi$  mesons, which have the lightest mass and longest range in the  $NN$  interaction. The important interaction for this process is  $K\pi$  scattering, which is not small at the relevant energies, and even has a low energy resonance,  $K^*(892)$ , which may play a role. Since the pion is virtual, it is important to take into account properly the off-shell behavior of the  $K\pi$  amplitude. The model we propose is a natural exten-

sion of our previous work on the MEC contributions to pion double charge exchange (DCX) scattering from nuclei [13,14].

We calculate the MEC amplitude for forward scattering,  $F^{\text{MEC}}$ , for  $K^+$  momenta  $400 \text{ MeV}/c < p < 1.2 \text{ GeV}/c$ , covering the range of recent experiments. We find  $\text{Im}(F^{\text{MEC}})$  (which gives the  $K^+$  total cross section) is determined with more certainty than  $\text{Re}(F^{\text{MEC}})$ , since the former is more constrained by unitarity and less dependent on the method of off-shell extrapolations. The model imposes a strong energy dependence (from unitarity) on  $\text{Im}(F^{\text{MEC}})$ , such that it must vanish below  $p \sim 400 \text{ MeV}/c$ . Well above this threshold (for  $\pi$  production),  $\text{Im}(F^{\text{MEC}})$  reaches a magnitude of about 6% of the predictions of multiple scattering theory. This gives a substantial improvement of the agreement of the total cross section given by scattering theory with the experimental results. We also predict an increase in the differential cross section at forward angles, of 10% or more (with considerable uncertainties).

Akulonichev [12] has given an estimate of  $\text{Im}(F^{\text{MEC}})$ , using an argument based on on-shell quantities only, and finding an effect on  $\sigma_t$  of  $\sim 10\%$ . Although the order of magnitude so obtained is not bad at the higher momenta, we find a number of differences between a fully off-shell theory and his method, such that the numerical similarities must be considered fortuitous. This is discussed in detail in Sec. V.

The paper is organized as follows. First is a presentation of the general theoretical framework for our MEC model in Sec. II. This is followed by calculations of forward amplitudes with numerical results in Sec. III. Section IV is devoted to a careful examination of the sources of uncertainties induced within our work. In Sec. V the importance of the main features of our model is discussed, including crossing symmetry and construction of the off-shell amplitude. An investigation of corrections for chiral symmetry follows. Comparisons of our results with experiment are given in Sec. VI, and conclusions are summarized in Sec. VII.

## II. THEORETICAL FRAMEWORK

In this section, we introduce the theoretical framework of our MEC model for the  $K^+$ -nucleus elastic scattering. As we show below, the model involves two important physical inputs: one is the momentum distribution of the pion exchange current in the nucleus and the other is the isoscalar  $K\pi$  scattering amplitude. To proceed, following a general introduction of the model, we first discuss calculations of the pion momentum distributions through which the importance of including realistic nuclear correlations in calculations is demonstrated. Using the results in Refs. [15–19], we also show some important features associated with the excess pion distribution. Then we discuss the construction of the off-shell  $K^+\pi$  scattering amplitude. For the energy region of interest, our  $K\pi$  model contains two parts consisting of a linear amplitude and a resonant amplitude. The former bears a strong resemblance to Weinberg's low energy  $\pi$  scattering model [20] while the latter is modeled on the resonant  $K\pi$

scattering data, both of which satisfy the crossing symmetry and elastic unitarity. Parameters in the  $K\pi$  model are fixed by using on-shell  $K\pi$  scattering data.

### A. Meson exchange current model for $K^+$ -nucleus scattering

For a nuclear target with total isospin  $I=0$ , the forward scattering amplitude for the interaction process represented by Fig. 1(a) can be written as

$$F^{\text{MEC}}(0) = -\frac{1}{4\pi} \int d\mathbf{q} \mathcal{M}_0^{K\pi}(\mathbf{p}, \mathbf{q}) W_A^\pi(\mathbf{q}) \quad (1)$$

where  $\mathcal{M}_0^{K\pi}(\mathbf{p}, \mathbf{q})$  stands for the isoscalar invariant amplitude for  $K\pi$  scattering and depends on  $\mathbf{p}$  and  $\mathbf{q}$ , the three-momenta of the kaon and pion, respectively. Here,  $W_A^\pi(\mathbf{q})$  is a momentum distribution function for the exchanged pions which can be derived by applying the rules of covariant perturbative theory (see also Refs. [13,14]). As we will show later, it is closely related to the distribution of excess pions defined by other authors (Refs. [15–19])

$$\delta n_A(\mathbf{q}) = \langle n(\mathbf{q}) \rangle_A - A \langle n(\mathbf{q}) \rangle_N, \quad (2)$$

where  $n(\mathbf{q})$  counts pions of momentum  $\mathbf{q}$ , and  $\langle \rangle_A, \langle \rangle_N$  refer to expectation values for the nuclear target, and a single nucleon. Then the average excess pion number  $\langle \delta n \rangle_A$  is given by the (dimensionless) integral

$$\overline{\langle \delta n \rangle_A} = \frac{\langle \delta n \rangle_A}{A} = \frac{1}{A} \int d\mathbf{q} \delta n_A(\mathbf{q}). \quad (3)$$

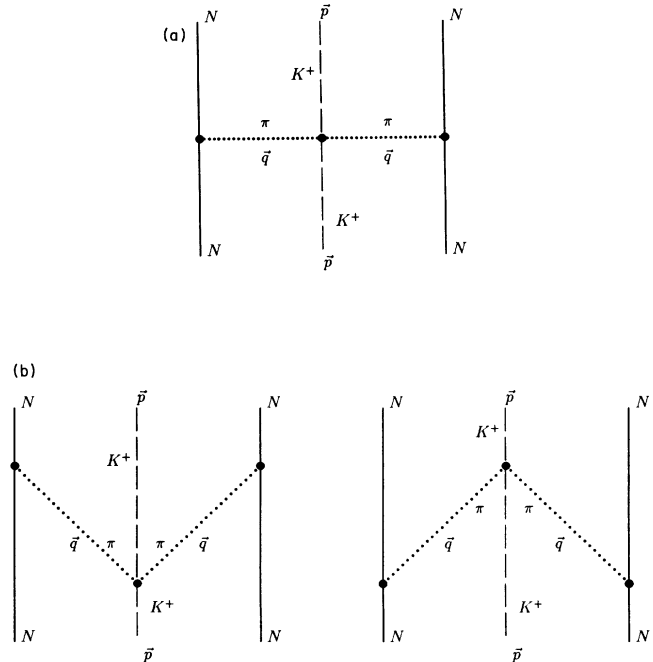


FIG. 1. (a) A general diagram of pion MEC contribution to the  $K^+$ -nucleus scattering; and (b) two time-ordered MEC diagrams [included in (a)] with a pair of pions created or annihilated in the  $K\pi$  scattering.

To agree with our definition given in Eq. (1), we shall find that the distributions are related by

$$W_A^\pi(\mathbf{q}) = \frac{\delta n_A(\mathbf{q})}{\mathcal{E}_\pi(q)}, \quad (4)$$

where  $\mathcal{E}_\pi(q)$  denotes the pion energy  $\sqrt{m_\pi^2 + q^2}$ . [We note that in the covariant formalism, the meson exchange processes include the two time-ordered diagrams of Fig. 1(b), with a pair of pions created or annihilated in the scattering. Without these contributions, the right-hand side of Eq. (4) would be reduced by  $\frac{1}{2}$ ; this counting effect has also been noted in Ref. [16].]

As seen from the above, there are two basic ingredients in the MEC model:  $\delta n_A(\mathbf{q})$  and  $\mathcal{M}_0^{K\pi}$ . Our knowledge about them will directly affect our understanding of the pion MEC contribution to the  $K^+$ -nucleus scattering. In the following two subsections, we discuss how to obtain these two quantities from available theoretical and experimental information.

### B. Pion excess and momentum distributions

Assuming that the nuclear state is described in terms of nucleon variables only, the pion momentum distribution required for Eq. (1) is then given by

$$W_A^\pi(\mathbf{q}) = \frac{g^2}{4M_N^2} \sum_{i < j}^A \frac{F^2(q)}{(2\pi)^3} \langle \psi_A | \frac{(\boldsymbol{\sigma}_i \cdot \mathbf{q})(\boldsymbol{\sigma}_j \cdot \mathbf{q})}{\mathcal{E}_\pi(q)^4} (\boldsymbol{\tau}_i \cdot \boldsymbol{\tau}_j) \exp(-i\mathbf{q} \cdot \mathbf{r}_{ij}) | \psi_A \rangle \quad (5)$$

where  $g$  and  $F$  are coupling constant ( $g = 13.5$ ) and form factor of the  $\pi N$  vertex,  $\psi_A$  is the nuclear target wave function in a static approximation, and  $\mathbf{r}_{ij}$  is the relative coordinate for nucleons  $i, j$ . [Compare Eq. (1) with Ref. [13], Eq. (11) evaluated at forward angle: however, the isospin factor is different for DCX.]

The pion excess distribution of Eq. (2) has been defined in Ref. [15] [see their Eqs. (5) and (6)] by an expression equivalent to Eqs. (4) and (5) for nucleonic wave functions. [The factor of  $\mathcal{E}_\pi(q)^{-1}$  in Eq. (4) may be thought of as arising from a frame transformation for the  $K\pi$  scattering: see Eq. (36).] Additional terms may be included in Eq. (5) for  $\Delta$ 's in the nuclear wave function, as described below. We continue our discussion in terms of  $\delta n(\mathbf{q})$  to make further connection with the work of Refs. [15–19].

Calculations of  $\delta n(\mathbf{q})$  using different assumptions about nuclear structure have shown that  $NN$  correlations induced by the nuclear tensor interaction play an extremely important role, determining not only the magnitude, but the *sign* of the excess pion number  $\langle \delta n \rangle_A$ . To illustrate this, we first calculate for spinless nuclei, such as  $^{12}\text{C}$  and  $^{40}\text{Ca}$  in their ground states, using shell model basis functions with no further correlations among nucleons. An explicit expression can be derived:

$$4\pi q^2 \delta n(q) = \frac{9}{\pi^2} \frac{g^2}{4M_N^2} \sum_{jj'} (2j+1)(2j'+1)(2l+1)(2l'+1) \sum_L (-1)^L q^4 \frac{[F(q^2) D_{ll'L}^{(jj')}(q)]^2}{\mathcal{E}_\pi(q)^3}, \quad (6)$$

where  $j$  and  $j'$  under  $\sum$  represent single particle orbits  $(nl)j$  and  $(n'l')j'$ . The nuclear structure information carrier  $D_{ll'L}^{(jj')}(q)$  is given by the recoupling expression

$$D_{ll'L}^{(jj')}(q) = \sum_\lambda (-1)^{\lambda/2} \sqrt{2\lambda+1} \begin{pmatrix} \frac{1}{2} & \frac{1}{2} & 1 \\ l & l' & \lambda \\ j & j' & L \end{pmatrix} (l'0, l0, \lambda 0)(10, \lambda 0, L 0) H_{\lambda ll'}(q) \quad (7)$$

with the multipole nuclear form factor  $H_{\lambda ll'}(q) = \int dr r^2 j_\lambda(qr) R_{nl}(r) R_{n'l'}(r)$  [13]. Note that  $\delta n(q)$  is isotropic because of the spinless target.

The numerical results are shown in Fig. 2 where the radial parameter  $\alpha$  of the harmonic oscillator wave function is chosen using  $\alpha = 0.5(1/A)^{1/3} \text{fm}^{-2}$ . As shown in Fig. 2, the calculation without correlations for  $^{12}\text{C}$  and  $^{40}\text{Ca}$  gives a negative distribution for all momenta shown, thus leading to a negative pion excess in nuclei. [The integrated average excess pion numbers  $\langle \delta n \rangle_A$  are  $-0.032$  ( $\Lambda = 3 \text{ fm}^{-1}$ ) and  $-0.041$  ( $\Lambda = 6 \text{ fm}^{-1}$ ) for  $^{12}\text{C}$ ; and  $-0.032$  and  $-0.040$  for  $^{40}\text{Ca}$  accordingly.] This feature is the same as shown in nuclear matter also using the lowest-order approximation (equivalent to the case without correlations, see  $N=2$  result of Table I of Ref. [15]). However, the negative pion excess is physically not correct, because of the neglect of tensor correlations, as

already indicated.

Calculations of  $\delta n(q)$  with the inclusion of tensor correlations have been done for nuclear matter and a number of finite nuclei, using realistic models of nuclear structure [15,19]. These authors include  $\Delta$  contributions to the pion excess, to be consistent with the meson-exchange  $NN$  interaction used for the nuclear structure. In contrast to the calculation without correlations, their complete result for the momentum distribution  $\delta n(q)$  possesses the following features: it is negative when  $q < 1 \text{ fm}^{-1}$  and becomes positive thereafter with a peak at around  $2 \text{ fm}^{-1}$  (see the solid curve of Fig. 2, which gives the result for  $^{56}\text{Fe}$  from Fig. 5 of Ref. [19(a)]). Jung and Miller [17], using a very different approach, have obtained a very similar result, supporting the calculations of Refs. [15,19]. Both calculations are based on conventional nuclear theory with correlations and  $\Delta$  contributions

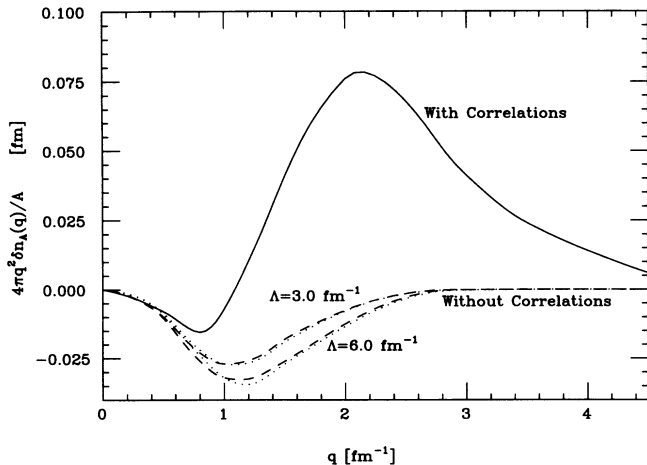


FIG. 2. Momentum distributions  $4\pi q^2 \delta n_A(q)/A$ : The solid curve is the result from Ref. [19(a)] for  $^{56}\text{Fe}$  with inclusion of correlations and  $\Delta$ . The dashed (dotted) curves are our results for  $^{40}\text{Ca}$  ( $^{12}\text{C}$ ) without correlations.  $\Lambda$  is the cutoff parameter of the  $\pi N$  vertex function.

included. At present, no other results from models beyond this conventional picture are available.

As remarked earlier, the sign of  $\langle \delta n \rangle_A$  in these complete calculations is positive. A qualitative argument for the sign is based on the similarity in structure between  $\delta n(\mathbf{q})$  and the one-pion exchange potential  $V_\pi(\mathbf{q}) = -\delta n(\mathbf{q}) \mathcal{E}_\pi(q)$ . Since the average of this potential in the target, including correlations, is expected to be negative  $\langle V_\pi \rangle < 0$ ,  $\langle \delta n \rangle_A$  must be positive [19(a)].

In this work we employ the momentum distribution  $\delta n(q)$  for  $^{56}\text{Fe}$  given in Ref. [19] as input data. Because the shape of the momentum distribution does not change dramatically for all but the lightest nuclei [19], we shall assume that except for a difference in an overall normalization, the momentum distributions for  $^{12}\text{C}$ ,  $^{40}\text{Ca}$ , and  $^{56}\text{Fe}$  have the same functional form. (This can also be seen in our calculation without correlations for  $^{12}\text{C}$  and

$^{40}\text{Ca}$ , as shown in Fig. 2. Sensitivity to changes in shape will be discussed in Sec. IV.) Then, the momentum distribution of pion excess in a finite nucleus ( $A$ ) can be expressed as

$$\delta n_A(\mathbf{q}) = \langle \delta n \rangle_A \rho_0(\mathbf{q}) \quad (8)$$

where we introduce a universal function  $\rho_0(\mathbf{q})$  which represents a normalized momentum distribution of pion excess with  $\int d\mathbf{q} \rho_0(\mathbf{q}) = 1$ . With this approximation  $\langle \delta n \rangle_A$  remains the only quantity which measures the  $A$  dependence of the MEC contributions to the  $K^+$ -nucleus scattering. The numerical values of  $\delta n$  and  $\rho_0$  are obtained using the results of Ref. [19(a)] and are listed in Table I.

Using Eq. (8), we can rewrite Eq. (1) as

$$F^{\text{MEC}}(0) = \langle \delta n \rangle_A f^{\text{MEC}}(0) \quad (9)$$

where the  $A$ -independent forward scattering amplitude is given by

$$f^{\text{MEC}}(0) = -\frac{1}{4\pi} \int d\mathbf{q} \mathcal{M}_0^{K\pi}(\mathbf{p}, \mathbf{q}) w(\mathbf{q}). \quad (10)$$

The new momentum distribution function  $w(\mathbf{q})$  is defined as

$$w(\mathbf{q}) = \frac{\rho_0(\mathbf{q})}{\mathcal{E}_\pi(q)}, \quad (11)$$

its numerical values are also shown in Table I.

### C. Isoscalar $K\pi$ invariant scattering amplitude

Let us start with the isospin tensor decomposition for the  $K\pi$  invariant amplitude

$$\mathcal{M}(K\pi) = \mathcal{M}_0(K\pi) + \mathcal{M}_1(K\pi) \left[ \mathbf{I}_\pi \cdot \frac{\boldsymbol{\tau}}{2} \right] \quad (12)$$

where  $\mathbf{I}_\pi$  and  $\boldsymbol{\tau}/2$  are isospin operators for pion and kaon,  $\mathcal{M}_0(K\pi)$  and  $\mathcal{M}_1(K\pi)$  are the isoscalar and isovector

TABLE I. Momentum distributions defined in Eqs. (8) and (11), with their integrated values.

$q$ ( $\text{fm}^{-1}$ )	$4\pi q^2 \delta n_A(q)/A$ (fm)	$4\pi q^2 \rho_0(q)$ (fm)	$4\pi q^2 w(q)$ ( $\text{fm}^2$ )
0.0	0.0	0.0	0.0
0.5	-0.008	-0.063	-0.073
1.0	-0.007	-0.055	-0.045
1.5	0.041	0.323	0.195
2.0	0.076	0.598	0.282
2.5	0.068	0.535	0.206
3.0	0.041	0.323	0.105
3.5	0.024	0.189	0.053
4.0	0.015	0.118	0.029
4.5	0.006	0.047	0.010
5.0	0.001	0.008	0.002
5.5	0.0001	0.0008	0.0001
6.0	0.0	0.0	0.0
	$\overline{\langle \delta n \rangle}_A = 0.13$	$\int \rho_0(\mathbf{q}) d\mathbf{q} = 1.0$	$\int w(\mathbf{q}) d\mathbf{q} = 0.37$

tor invariant amplitudes, respectively, and can be expressed in terms of the isospin amplitudes  $T_I$ , with  $I = \frac{1}{2}, \frac{3}{2}$  for  $K\pi$ :

$$\begin{aligned}\mathcal{M}_0 &= \frac{1}{3}[2T_{3/2} + T_{1/2}], \\ \mathcal{M}_1 &= \frac{2}{3}[T_{3/2} - T_{1/2}].\end{aligned}\quad (13)$$

Direct experimental results for  $K\pi$  scattering are not available. However, there are some indirect measurements which make use of the analysis of the  $KN \rightarrow KN\pi$  reaction from which phenomenological  $K\pi$  phase shifts can be derived. We use data from the analysis of Estabrooks *et al.* [21], who found that for  $\sqrt{s_{K\pi}} < 1$  GeV the dominant contributions are from  $s$  and  $p$  waves and all other higher partial waves are negligible. As a result, the on-shell invariant amplitude in the partial-wave representation can be written as

$$T_I^L(s) = -8\pi\sqrt{s} \frac{2L+1}{D_I^L(s) - ik}, \quad L=0,1, \quad (14)$$

with  $D_I^L(s) = k \cot \delta_{2I}^L$ , where  $s$  and  $k$  are the total energy squared and the momentum in the c.m. frame, satisfying the following relativistic relation:

$$k = \left[ \frac{[s - (m_\pi + m_k)^2][s - (m_\pi - m_k)^2]}{4s} \right]^{1/2}. \quad (15)$$

In the above  $\delta_{2I}^L$  is the phase shift. For  $L=0$ , it is parametrized using effective range form

$$D_I^0(s) = \frac{1}{a_{2I}} + \frac{1}{2}r_{2I}k^2 \quad (16)$$

with parameters given in Ref. [21]:  $a_3 = -1.00$ ,  $a_1 = 2.39$ , and  $r_3 = r_1 = -1.76$  [all in  $(\text{GeV}/c)^{-1}$ ]. The  $p$  wave is dominated by an  $I = \frac{1}{2}$  resonance,  $K^*(892)$ , which is therefore fit by the resonant form:

$$\frac{k}{D_{1/2}^1(s) - ik} = \frac{M_r \Gamma(k)}{M_r^2 - s - iM_r \Gamma(k)}, \quad (17)$$

where

$$\Gamma(k) = \left[ \frac{k}{k_r} \right]^3 \Gamma_r \left[ \frac{1 + (k_r R)^2}{1 + (kR)^2} \right] \quad (18)$$

with parameters [21]  $M_r = 895.7$  MeV,  $\Gamma_r = 52.9$  MeV,  $R = 4.3$   $(\text{GeV}/c)^{-1}$ .  $k_r$  is the resonant c.m. momentum which can be obtained from  $M_r$ , using Eq. (15). The  $I = \frac{3}{2}$   $p$  wave is negligible. (We do not include experimental uncertainties in our calculations.)

The above information about  $K\pi$  scattering provides us with an on-shell constraint on the  $K\pi$  invariant amplitude. However, because the virtual pion under consideration is far off its mass shell, we also need guidelines for carrying out an off-shell continuation of the  $K\pi$  invariant amplitude. In the following, we proceed to construct an isoscalar amplitude which is consistent with unitarity and crossing symmetry, using the on-shell data to help fix its parameters.

We shall express the  $K\pi$  invariant amplitude  $\mathcal{M}_0^{K\pi}$  in

Eq. (1) in terms of the Mandelstam variables  $s, t, u$ , and the momenta  $k(s), k(u)$  corresponding to  $s, u$ . We first introduce a term which represents the nonresonant  $s$ - and  $p$ -wave  $K\pi$  scattering at low energy. For this domain we consider an expansion only to linear order in these kinematic variables, which is in close analogy to the approach used in low energy  $\pi\pi$  scattering [20]. Crossing symmetry requires that the isoscalar  $K\pi$  amplitude be even under the interchange  $s \leftrightarrow u$ . Therefore, the linear expansion takes the form

$$\mathcal{M}_0^{\text{lin}} = \alpha_0 + \beta_0(s+u) + i\beta'_0[k(s) + k(u)], \quad (19)$$

where  $\alpha_0, \beta_0, \beta'_0$  are real constants. We omit a term linear in  $t$ , which will vanish for forward scattering. With the last ( $\beta'_0$ ) term omitted, Eq. (19) corresponds to the Weinberg form for  $\pi X$  isoscalar scattering at very low energy [20]. The  $\beta'_0$  term is required by minimal elastic unitarity, and will be important for our present application. For given  $x$  ( $x = s$  or  $u$ ),  $k(x)$  in Eq. (19) is calculated using a threshold (nonrelativistic) expansion form

$$k(x) = \frac{\sqrt{m_\pi m_k}}{m_\pi + m_k} \sqrt{x - (m_\pi + m_k)^2}, \quad (20)$$

which is consistent with the threshold feature of the linear model. This expansion is employed to remove an unphysical region and pole in Eq. (15) when extrapolating to off-shell values of  $x < (m_\pi + m_k)^2$ , as discussed later in the context of unitarity.

The second part of our model consists of a resonant scattering term:

$$\begin{aligned}\mathcal{M}_0^{\text{res}}(s, t, u) &= \left[ T_{\text{res}}(s) \left[ 1 + \frac{t}{2k(s)^2} \right] \theta(s - x_0) \right. \\ &\quad \left. + T_{\text{res}}(u) \left[ 1 + \frac{t}{2k(u)^2} \right] \theta(u - x_0) \right] \quad (21)\end{aligned}$$

with

$$T_{\text{res}}(x) = \frac{8\pi\sqrt{x}}{k(x)} \frac{M_r \Gamma(k(x))}{M_r^2 - x - iM_r \Gamma(k(x))}, \quad (22)$$

and where  $x = s$  or  $u$ , and  $x_0 = (m_\pi + m_k)^2$  is the (squared) threshold energy for physical  $K\pi$  scattering. The  $t$  dependence of Eq. (21) gives the  $p$ -wave angular dependence on-shell, and the step functions  $\theta(x - x_0)$  restrict the resonant amplitudes to  $s$  and  $u$  above threshold. As a result, the resonant scattering amplitude has no unphysical poles below threshold. (Note that  $\mathcal{M}_0^{\text{res}}$  has fully relativistic kinematics, while in  $\mathcal{M}_0^{\text{lin}}$ , some nonrelativistic approximations are used.)

Putting the above two terms [Eqs. (19) and (21)] together, our model off-shell amplitude becomes

$$\mathcal{M}_0(s, t, u) = \mathcal{M}_0^{\text{lin}} + \mathcal{M}_0^{\text{res}}, \quad (23)$$

which can be seen to be explicitly crossing symmetric. Considerations of unitarity imply that the amplitude should have an imaginary part only if  $s$  or  $u$  is above

threshold. This will obtain for Eq. (19), provided the momenta  $k(x)$  are real for  $x > x_0$ , and imaginary for  $x < x_0$ . This physical requirement is well observed by the expansion form of  $k(x)$  in Eq. (20). [Note that the full relativistic function of Eq. (15) has a more complicated square-root structure.] Similarly, for the resonant amplitude of Eq. (21), the step functions also guarantee the unitarity behavior, by cutting off the amplitudes below threshold (at the expense of analyticity).

As we see from the above, the parameters of  $\mathcal{M}_0^{\text{res}}$  are completely fixed by the on-shell constraint. [The  $T_{\text{res}}(u)$  term vanishes for the on-shell  $K\pi$  kinematics.] Therefore, the only undetermined parameters in our model are those in  $\mathcal{M}_0^{\text{lin}}$ , and are determined by fitting the  $s$ -wave on-shell data, as follows. All quantities in Eq. (14) are expanded in power of  $k$ , using Eq. (16) with the effective range parameters given, and the inverse of Eq. (20)

$$\begin{aligned} \sqrt{x} &= (m_\pi + m_k) + \frac{(m_\pi + m_k)}{2m_\pi m_k} k^2(x) \\ &= (m_\pi + m_k) + \frac{k^2(x)}{2\mu} \end{aligned} \quad (24)$$

where  $\mu$  is the reduced mass of  $K\pi$  system. Only terms through  $k^2$  will be kept. Similarly,  $\mathcal{M}_0^{\text{lin}}$  of Eq. (19) is also expanded in powers of  $k = k(s)$ : this requires that  $u$  and  $k(u)$  be expanded in  $k$ , using on-shell kinematics. Then, matching coefficients of  $\mathcal{M}_0^{\text{lin}}$  and  $\frac{1}{3}[2T_{3/2}^0 + T_{1/2}^0]$  through order  $k^2$ , we obtain these equations

$$\begin{aligned} \alpha_0 + 2\beta_0(m_\pi^2 + m_k^2) - 2\mu\beta'_0 &= -\frac{8\pi(m_\pi + m_k)}{3} [a_1 + 2a_3], \\ \beta_0 &= \mu\beta'_0 \frac{m_\pi^2 + m_k^2}{8m_\pi^2 m_k^2} - \frac{2\pi}{3\mu} [a_1 + 2a_3] \\ &\quad + \frac{2\pi(m_\pi + m_k)}{3} [(a_1)^2 r_1 + 2(a_3)^2 r_3], \\ \beta'_0 &= -\frac{8\pi(m_\pi + m_k)}{3} [(a_1)^2 + 2(a_3)^2], \end{aligned} \quad (25)$$

which may be directly solved for the parameters  $(\alpha_0, \beta_0, \beta'_0)$ :

$$\begin{aligned} \alpha_0 &= -\frac{4\pi}{3} (m_\pi + m_k) (m_\pi^2 + m_k^2) [(a_1)^2 r_1 + 2(a_3)^2 r_3] \\ &\quad + \frac{2\pi}{3} \left[ \frac{(m_\pi^2 + m_k^2)^2}{m_\pi m_k} - 8m_\pi m_k \right] [(a_1)^2 + 2(a_3)^2] \\ &\quad + \frac{4\pi}{3} (m_\pi + m_k) \frac{(m_\pi - m_k)^2}{m_\pi m_k} [a_1 + 2a_3], \end{aligned}$$

TABLE II. Expansion parameters from different off-shell extrapolations of the linear  $K\pi$  amplitude, Eq. (19): (I), from Eq. (26); (II) and (III), see Sec. IV B.

	(I)	(II)	(III)
$\alpha_0$	18.7	11.4	-11.0
$\beta_0(\text{fm}^2)$	-2.2	-1.0	0.0
$\beta'_0(\text{fm})$	-8.1	-8.1	-8.1

$$\begin{aligned} \beta_0 &= \frac{2\pi}{3} (m_\pi + m_k) [(a_1)^2 r_1 + 2(a_3)^2 r_3] - \frac{\pi}{3} \frac{m_\pi^2 + m_k^2}{m_\pi m_k} \\ &\quad \times [(a_1)^2 + 2(a_3)^2] - \frac{2\pi}{3} \frac{m_\pi + m_k}{m_\pi m_k} [a_1 + 2a_3], \end{aligned} \quad (26)$$

$$\beta'_0 = -\frac{8\pi(m_\pi + m_k)}{3} [(a_1)^2 + 2(a_3)^2].$$

Their numerical values are listed in Table II (I), calculated using the parameters given after Eq. (16).

Therefore, applying general considerations of unitarity and crossing symmetry, we have constructed a model of the off-shell isoscalar invariant amplitude for  $K\pi$  scattering which has the correct behavior on-shell: for the  $s$  wave, at low energies, and for the  $p$  wave, near the  $K^*(892)$  resonance. The forward amplitude, given by Eq. (23) with  $t=0$ , is then to be used in Eqs. (1) or (10) for the calculation of  $F^{\text{MEC}}$ .

### III. CALCULATION OF MEC AMPLITUDES

We combine Eqs. (9)–(11), Eq. (19), Eq. (21), and Eq. (23) to obtain explicit expressions for the pion MEC contribution to the  $K^+ -^{12}\text{C}$  scattering. First we express the kinematic variables  $s$  and  $u$  in terms of the momenta  $\mathbf{p}, \mathbf{q}$  of the kaon and virtual pion [off shell:  $q_\mu = (0, \mathbf{q})$  in the static approximation]:

$$\begin{aligned} s &= m_k^2 - \mathbf{q}^2 - 2qp \cos\theta, \\ u &= m_k^2 - \mathbf{q}^2 + 2qp \cos\theta. \end{aligned} \quad (27)$$

Then  $k(s)$  and  $k(u)$  in  $\mathcal{M}_0^{\text{lin}}[\mathcal{M}_0^{\text{res}}]$  are obtained from Eq. (20) [Eq. (15)]. The forward amplitude per unit pion [Eq. (10)] can be separated into real and imaginary parts:

$$\begin{aligned} \text{Re}[f^{\text{MEC}}(0)] &= -\frac{1}{4\pi} \left[ [\alpha_0 + 2\beta_0(m_k^2 + m_\pi^2)] \int d\mathbf{q} w(q) - 2\beta_0 \int d\mathbf{q} (q^2 + m_\pi^2) w(q) \right. \\ &\quad \left. - \beta'_0 \int d\mathbf{q} w(q) [\text{Im}(k(s))\theta(x_0 - s) + \text{Im}(k(u))\theta(x_0 - u)] \right. \\ &\quad \left. + \int d\mathbf{q} w(q) [\text{Re}(T_{\text{res}}(s))\theta(s - x_0) + \text{Re}(T_{\text{res}}(u))\theta(u - x_0)] \right], \end{aligned} \quad (28a)$$

$$\begin{aligned} \text{Im}[f^{\text{MEC}}(0)] = & -\frac{\beta'_0}{4\pi} \int d\mathbf{q} w(q) [k(s)\theta(s-x_0) + k(u)\theta(u-x_0)] \\ & -\frac{1}{4\pi} \int d\mathbf{q} w(q) [\text{Im}(T_{\text{res}}(s))\theta(s-x_0) + \text{Im}(T_{\text{res}}(u))\theta(u-x_0)]. \end{aligned} \quad (28b)$$

From Eq. (28) one sees immediately that  $\text{Im}(f^{\text{MEC}})$  involves only integrals for  $s$  or  $u$  above threshold, while  $\text{Re}(f^{\text{MEC}})$  includes integrations over all pion momenta. For a given distribution  $w(q)$ , the actual amplitudes  $\text{Re}(F^{\text{MEC}})$ ,  $\text{Im}(F^{\text{MEC}})$  are obtained from Eq. (28) by scaling with  $\langle \delta n \rangle_A$ , as in Eq. (9).

Numerical results for  $^{12}\text{C}$  are given in Table III. We have used the pion density distribution  $w(q)$  given in Table I, obtained as described from Ref. [19(a)]. The values of  $\text{Re}(f^{\text{MEC}})$  and  $\text{Im}(f^{\text{MEC}})$  are obtained by integrating Eq. (28). These are then multiplied by a value of  $\langle \delta n \rangle_A$  appropriate for  $^{12}\text{C}$  to obtain  $F^{\text{MEC}}$ . We adopt a value of  $\langle \delta n \rangle_A/A = 0.1$  which interpolates between the values given in Ref. [15] for  $^4\text{He}$  (0.09) and  $^{27}\text{Al}$  (0.11), to obtain  $\langle \delta n \rangle_A = 1.2$  for  $^{12}\text{C}$ , which is used in Table III. This value may be considered an average result: uncertainties in  $\langle \delta n \rangle_A$  are discussed in the next section.

The results for  $F^{\text{MEC}}$  listed in column (a) are for the full model of the  $K\pi$  amplitude of the previous section, as given in Eq. (23). For comparison, column (b) gives the results with the resonant ( $p$ -wave)  $\mathcal{M}_0^{\text{res}}$  contributions omitted. It is clear that the resonance is quite important at higher energy for  $\text{Im}(F^{\text{MEC}})$ , although it has negligible effects on  $\text{Re}(F^{\text{MEC}})$ . At  $p = 1.2$  GeV, the contributions [to  $\text{Im}(F^{\text{MEC}})$ ] of the resonant (“ $p$ -wave”) terms are about 1.5 times as large as those of the linear (“ $s$ -wave”) terms. In column (c) we show the effect of omitting the contribution of the effective range terms, by setting  $r_1^0 = r_3^0 = 0$  in Eq. (26). We also omit the resonant terms so that amplitudes in (c) are generated entirely by the  $K\pi$  scattering lengths. The omission of the effective range terms only affects  $\text{Re}(F^{\text{MEC}})$ , as is clear from Eqs. (26) and (28); the effect is moderate.

Two features of the model for  $\text{Im}(F^{\text{MEC}})$  are apparent from Table III; and follow from the form given in Eq. (28b): (1) There is a threshold at  $p \sim 400$  MeV/ $c$ , and (2)  $\text{Im}(F^{\text{MEC}})$  increases monotonically with  $p$ . The first

comes from the  $K\pi$  kinematics with the pion off-shell: since  $s > x_0$  and  $u > x_0$ , one finds easily from Eq. (27) that the threshold occurs at

$$p = \sqrt{m_\pi^2 + 2m_k m_\pi} \sim 400 \text{ MeV}/c. \quad (29)$$

This is essentially the threshold for pion production on the nuclear target  $K^+ + ^{12}\text{C} \rightarrow K + \pi + ^{12}\text{C}$  (static approximation—no target recoil), as we would expect, since  $\text{Im}(F^{\text{MEC}})$  reflects (through unitarity) “knockout” of virtual pions from the target. The increase of  $\text{Im}(F^{\text{MEC}})$  with  $p$  is partly due to the increase in phase space, partly due to the increase in  $k(s)$ ,  $k(u)$ , and of the resonant terms, all with  $p$ .

We can see directly from Eq. (28) that within our theoretical approach, there is less uncertainty for the prediction of  $\text{Im}(F^{\text{MEC}})$  than for  $\text{Re}(F^{\text{MEC}})$ , given the on-shell data for  $K\pi$  scattering. This is due to the fact that  $\text{Im}(F^{\text{MEC}})$  is uniquely determined by the minimal unitarity condition and the on-shell data while  $\text{Re}(F^{\text{MEC}})$  depends also on the off-shell continuation of the  $K\pi$  amplitude. Actually, in the present model, the main uncertainty in  $\text{Im}(F^{\text{MEC}})$  comes from the (excess) pion distribution. As we shall see in the next section, with some possible uncertainty in scale to be fixed by  $\langle \delta n \rangle_A$ , our values for  $\text{Im}(F^{\text{MEC}})$  are reasonably firm. On the contrary,  $\text{Re}(F^{\text{MEC}})$  will bear many more uncertainties. We will also learn that the inclusion of crossing symmetry is important to our result.

#### IV. SOURCES OF UNCERTAINTIES

This section discusses the sources of uncertainty; they included the excess pion distribution expressed in  $W(q)$ , which mostly affects the overall scale of  $F^{\text{MEC}}$ ; the treatment of the off-shell extrapolation of the  $K\pi$  amplitude; and the integration over kinematics below threshold. As we have just discussed, this latter does not affect

TABLE III. The MEC  $K^+ - ^{12}\text{C}$  forward scattering amplitudes (in units of fm) for different model assumptions;  $f^{\text{MEC}}$  and  $F^{\text{MEC}}$  (a) are the results of our full model in Eq. (28), (b) gives contribution of  $\mathcal{M}_0^{\text{lin}}$  only, (c) same, in scattering length approximation.

$p$ (MeV/ $c$ )	$f^{\text{MEC}}(0)$ $\langle \delta n \rangle_A = 1.0$		$F^{\text{MEC}}(a)$ $\langle \delta n \rangle_A = 1.2$		$F^{\text{MEC}}(b)$ $\langle \delta n \rangle_A = 1.2$		$F^{\text{MEC}}(c)$ $\langle \delta n \rangle_A = 1.2$	
	$\text{Re}(f)$	$\text{Im}(f)$	$\text{Re}(F)$	$\text{Im}(F)$	$\text{Re}(F)$	$\text{Im}(F)$	$\text{Re}(F)$	$\text{Im}(F)$
400	-1.24	0.0	-1.49	0.0	-1.49	0.0	-1.12	0.0
500	-1.20	0.02	-1.44	0.02	-1.45	0.02	-1.09	0.02
600	-1.16	0.05	-1.39	0.06	-1.43	0.06	-1.07	0.06
700	-1.09	0.09	-1.31	0.11	-1.42	0.09	-1.06	0.09
800	-1.02	0.21	-1.22	0.25	-1.42	0.13	-1.06	0.13
900	-1.03	0.34	-1.24	0.41	-1.42	0.16	-1.06	0.16
1000	-1.09	0.44	-1.31	0.52	-1.43	0.19	-1.06	0.19
1100	-1.15	0.50	-1.38	0.59	-1.43	0.22	-1.07	0.22
1200	-1.22	0.53	-1.46	0.64	-1.44	0.25	-1.07	0.25

$\text{Im}(F^{\text{MEC}})$ , although it can be quite important for  $\text{Re}(F^{\text{MEC}})$ .

### A. Excess pion momentum distribution

The amplitude  $F^{\text{MEC}}$  depends on the momentum distribution  $W_A(q)$  [or equivalently,  $\delta n(q)$ ], through both the functional form and the scale given by the pion excess number  $\langle \delta n \rangle_A$ . The strongest characteristic of  $\delta n(q)$  is the change of sign from negative values for  $q \leq 1 \text{ fm}^{-1}$  to positive values, peaking at  $q \sim 2 \text{ fm}^{-1}$ . This feature is given by all models which incorporate tensor correlations from the  $NN$  interaction into the nuclear wave function [15–17,19]. Details of the shape change with different models, as can be seen, e.g., in Fig. 2(a) of Ref. [17(b)], which compares their values of  $\delta n(q)$  with those of Ref. [19(b)]. These two cases are very similar in shape, presumably because they have similar dynamical input. Even so, the small differences give a 10% difference in the values of  $\langle \delta n \rangle$ .

Differences in dynamical models tend to change the relative weight of high- and low-momentum components, which is amplified in the change of integrated value of  $\langle \delta n \rangle_A$ . Thus, two different models for including the  $\Delta$  component in nuclei [19] give a variation in  $\langle \delta n \rangle_A$  by a factor of 0.73 for the same nuclei. On the other hand, models [17,19] which include the  $\Delta$  have larger higher-momentum components than those based only on  $NN$  correlations [16,19], and therefore larger values of  $\langle \delta n \rangle_A$ .

To test for the sensitivity of the amplitude  $F^{\text{MEC}}$  to the pion momentum distribution, we perform two kinds of calculation. First, we vary the cutoff parameters  $\Lambda$  in the pion vertex function

$$F(q, \Lambda) = \left( \frac{\Lambda^2 - m_\pi^2}{\Lambda^2 + q^2} \right)^2. \quad (30)$$

Reference [19] uses the value  $\Lambda_0 = 7.0 \text{ fm}^{-1}$ ; varying this value changes the shape of the momentum distribution by

$$\delta n'_A(q) = \delta n_A(q) \left( \frac{F(q, \Lambda)}{F(q, \Lambda_0)} \right)^2. \quad (31)$$

The largest changes are at the highest momenta. In Fig. 3 we show the variation of  $F^{\text{MEC}}$  for three values of  $\Lambda$ : 7.0 [=  $\Lambda_0$ ; same as Table III(a)], 6.0, and 4.5  $\text{fm}^{-1}$ . As shown in the figure,  $F^{\text{MEC}}$  decrease with smaller (softer) values of  $\Lambda$ , but so do the values of the average excess pion number, which are 0.10, 0.08, and 0.05 accordingly. We note that the variation of  $F^{\text{MEC}}$  approximately scales with  $\langle \delta n \rangle_A$ : in fact  $\text{Im}(F^{\text{MEC}})$  changes less than linearly with  $\langle \delta n \rangle_A$ , presumably because it is less weighted by the low-momentum values of  $\delta n(q)$ .

We also tested the sensitivity of  $F^{\text{MEC}}$  to change of the momentum distribution by shifting the argument  $q$  in  $q^2 \delta n(q)$  by a constant momentum:  $q \rightarrow q - \Delta q$ ; this shifts the peak by  $\Delta q$  without changing the value of  $\langle \delta n \rangle_A$ . For shifts ( $\Delta q = 0.25, 0.5 \text{ fm}^{-1}$ ) which correspond to increases of 10% and 20% in the peak position, the changes in  $\text{Re}(F^{\text{MEC}})$  are comparable. For  $\text{Im}(F^{\text{MEC}})$

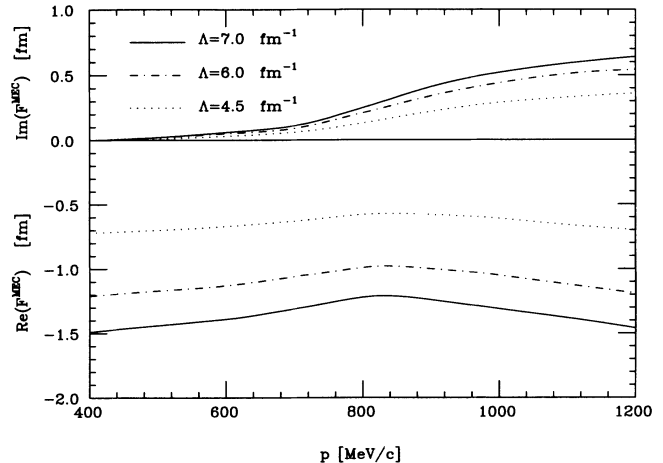


FIG. 3. Sensitivity of the real and imaginary MEC amplitudes to the cutoff parameter  $\Lambda$  in  $\delta n^\pi(q)$ . The excess pion numbers per nucleon for  $\Lambda = 7.0, 6.0,$  and  $4.5 \text{ fm}^{-1}$  are 0.10, 0.08, and 0.05 accordingly.

there is very little change for  $p \leq 900 \text{ MeV}/c$ , and small *negative* changes for higher values of  $p$ . (These reflect changes in the balance between the resonant and non-resonant  $K\pi$  amplitudes.)

We conclude that the largest uncertainty in our calculated amplitudes [particularly for  $\text{Im}(F^{\text{MEC}})$ ] from the momentum distribution are connected to the uncertainty in the scale, characterized by the pion excess number  $\langle \delta n \rangle_A$ . As we have discussed, various models [15–19] give values (per nucleon) of  $\langle \delta n \rangle_A \sim 0.07\text{--}0.13$ , or  $\langle \delta n \rangle_A \sim 0.8\text{--}1.5$  for  $^{12}\text{C}$ , which gives us an estimate of the uncertainty in  $F^{\text{MEC}}$ .

### B. Off-shell extrapolation of $K\pi$ amplitude

Our calculations have been done in terms of a model for the isoscalar  $K\pi$  invariant amplitude whose form is given in Eq. (23). The form of the resonant amplitude is fairly standard, and will not be discussed further. The “linear” amplitude of Eq. (19) keeps the lowest orders in the kinematics variables, the parameters of which are fixed from the effective range parameters, as in Eqs. (25) and (26). In this subsection we explore what freedoms exist to vary the form of Eq. (19), still constrained by on-shell data.

The first point is that  $\beta'_0$  is fixed by unitarity in the form shown in Eq. (26), so there is no further freedom in the imaginary amplitude  $\text{Im}(\mathcal{M}_0)$ , and therefore  $\text{Im}(F^{\text{MEC}})$ . However,  $\beta'_0$  also influences  $\text{Re}(\mathcal{M}_0)[\text{Re}(F^{\text{MEC}})]$  for values of  $s$  or  $u < x_0$ , for which  $k(s)$  or  $k(u)$  are imaginary. This is shown in Fig. 4: (I) stands for  $\text{Re}(F^{\text{MEC}})$  for the full model [Table II (I)] while (IV) represents the contribution of the  $\beta'_0$  term of Eq. (28a); the latter is about 50% of the full  $\text{Re}(F^{\text{MEC}})$ .

This contribution would be eliminated if we changed Eq. (19) by requiring that the  $\beta'_0$  term contribute only above threshold ( $s, u > x_0$ ), thus eliminating the  $\beta'_0$  term in Eq. (28a). However, this also changes the values of  $\alpha_0$  and  $\beta_0$ , since Eq. (25) must also be altered by removing  $\beta'_0$

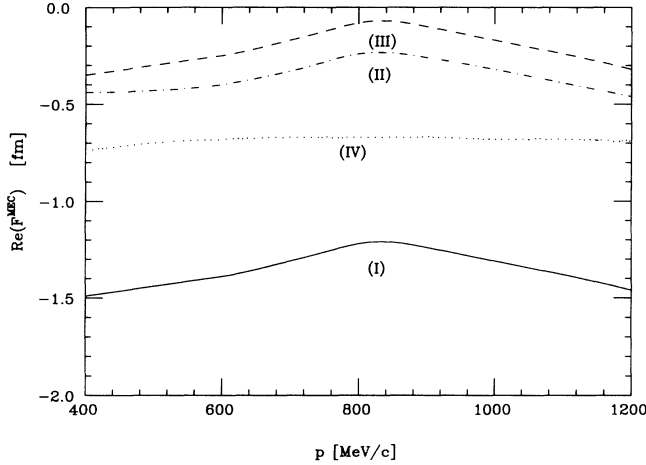


FIG. 4. Sensitivity of  $\text{Re}(F^{\text{MEC}})$  to different off-shell extrapolations: (I) full model, (II) no  $\beta'_0$  contribution, (III)  $\beta_0=0$ , (IV)  $\beta'_0$  contribution alone; see text.

in the first two equations. The corresponding numerical values for  $\alpha_0$ ,  $\beta_0$ , and  $\beta'_0$  are given in Table II (II); they differ largely from those of the full model (I), though there is no sign change. The result of these changes on  $\text{Re}(F^{\text{MEC}})$  is shown in Fig. 4 (II). As expected, they are quite different from those of (I), and are not given by the difference (I)–(IV) either. The point here is that different values for extrapolating terms in  $k(s), k(u)$  from the physical region (real values) to the unphysical region (imaginary values) make large differences for  $\text{Re}(F^{\text{MEC}})$ , but not for  $\text{Im}(F^{\text{MEC}})$ .

Another possible change of extrapolation is the elimination of the  $(s+u)$  term of Eq. (19) by setting  $\beta_0=0$ . [This is equivalent to replacing  $(s+u)$  by  $2(m_\pi^2+m_K^2)-t$ , which will agree on-shell: however, since  $t=0$  for forward amplitudes, the altered term becomes a constant.] Again, Eq. (25) must be modified: the second equation is dropped, leaving the (last) equation for  $\beta'_0$  unchanged, and the value of  $\alpha_0$  determined by the first equation, with  $\beta_0=0$ . (See Table II for the numerical value for  $\alpha_0$ .)  $\text{Re}(F^{\text{MEC}})$  for this extrapolation is shown in Fig. 4 (III). The results are surprisingly close to those of (II), although the changes from the original model (I) result from different terms in Eq. (28a).

To summarize, we have shown that the on-shell information on the  $K\pi$  amplitudes does not fully constrain the real part of the off-shell amplitude, even for an expansion similar to that introduced in Sec. II. Within the range of possibilities just discussed, we find the magnitude and sign:  $\text{Re}(F^{\text{MEC}}) \sim -0.5 \text{ fm}^{-1}$ . However, keeping to the orders given in Eq. (19), there is no freedom in the imaginary amplitudes.

We have not assessed the contribution to the uncertainties of our results resulting from those in the input  $K\pi$  data, since there does not seem to be a reliable way to do this. One could simply test the sensitivity to the quoted errors in Ref. [21] which are smaller than other uncertainties in our work; however, there are also variations in quoted values of parameters from other analyses (e.g.,

Ref. [22]). For the present application, it appears to be more sensible to use data with maximum available information (e.g.,  $s$  and  $p$  waves, the energy dependence, etc.) from one experiment, for consistency in decomposing the scattering amplitude.

## V. DISCUSSION

### A. Importance of crossing symmetry

In this subsection we demonstrate the importance of the crossing symmetry of the  $K\pi$  amplitude to the calculation of  $F^{\text{MEC}}$ . For comparison we introduce a simpler model which ignores the constraint of crossing symmetry, as follows. Take the  $K\pi$  invariant amplitude for forward scattering to be a function of  $s$  alone, with an expansion in partial waves:

$$\mathcal{M}_0(s) = \sum_L \left[ \frac{2}{3} T_{3/2}^L(s) + \frac{1}{3} T_{1/2}^L(s) \right]. \quad (32)$$

The  $T_l^L(s)$  are defined in Eq. (14) as functions of  $s$  [or  $k(s)$ ] determined by the on-shell data. Then  $s$  is given by Eq. (27) for integration of the amplitude over  $\mathbf{q}$ , as in Eq. (10).

There are immediate problems with the treatment of  $\sqrt{s}$  and  $k(s)$  extrapolated below threshold, due to square-root singularities, as well as unphysical poles generated by the effective range expansion. As in the method of Sec. II C, these difficulties can be avoided by expanding Eq. (14) in powers of  $k$  and setting the factor  $\sqrt{s} = (m_\pi + m_k)$ , i.e., its threshold value in the linear model; and by introducing a step function  $\theta(s-x_0)$  in the resonant term. With these approximations, Eq. (32) becomes

$$\begin{aligned} \mathcal{M}_0(s) = & -\frac{8\pi(m_\pi + m_k)}{3} \\ & \times \{ a_1^0 + 2a_3^0 - \frac{1}{2}k^2[(a_1^0)^2 r_1^0 + 2(a_3^0)^2 r_3^0] \\ & + ik[(a_1^0)^2 + 2(a_3^0)^2] \} \\ & - \frac{8\pi\sqrt{s}}{k} \frac{M_r \Gamma(k)}{M_r^2 - s - iM_r \Gamma(k)} \theta(s-x_0). \end{aligned} \quad (33)$$

Direct comparison with Eqs. (19) and (21) shows that for the forward imaginary amplitudes,

$$\text{Im}[\mathcal{M}_0(s, u)] = \text{Im}[\mathcal{M}_0(s) + \mathcal{M}_0(u)]. \quad (34)$$

Then integration over  $\mathbf{q}$  [using Eq. (27)] gives equal contributions from  $\text{Im}[\mathcal{M}_0(s)]$  and  $\text{Im}[\mathcal{M}_0(u)]$  to  $\text{Im}(F^{\text{MEC}})$ . The result is that neglect of crossing symmetry *omits* one-half the contribution to  $\text{Im}(F^{\text{MEC}})$ , even though both models have been fit to the same on-shell data. (The point is that  $\text{Im}[\mathcal{M}_0(u)]=0$  for on-shell  $K\pi$  scattering, but does contribute equally for virtual pions.) The numerical results shown in Table IV are evidence of the above expectation, where results of the *full model* are the same as that in Table III(a) and those under *off-shell* are from Eq. (33) without crossing symmetry.

The omission of crossing also reduces the values of

TABLE IV. The MEC amplitudes (in units of fm) from the model without crossing symmetry, Eq. (33) with off-shell and on-shell kinematics, compared with the full model. See Sec. V B.

$p$ (MeV/c)	Full model		Off-shell		On-shell	
	Re( $F$ )	Im( $F$ )	Re( $F$ )	Im( $F$ )	Re( $F$ )	Im( $F$ )
400	-1.49	0.0	-0.39	0.0	0.03	1.06
500	-1.44	0.02	-0.37	0.01	-0.04	0.98
600	-1.39	0.06	-0.34	0.03	-0.07	0.92
700	-1.31	0.11	-0.30	0.06	-0.07	0.86
800	-1.22	0.25	-0.26	0.13	-0.05	0.83
900	-1.24	0.41	-0.27	0.20	-0.02	0.80
1000	-1.31	0.52	-0.30	0.26	0.01	0.79
1100	-1.38	0.59	-0.34	0.30	0.04	0.79
1200	-1.46	0.64	-0.37	0.32	0.08	0.79

$\text{Re}(F^{\text{MEC}})$ , but not by a simple factor of 2 (see Table IV). This can be understood by the discussion given in the preceding section, resulting from a different off-shell extrapolation.

### B. On-shell approximation

Suppose the dependence of  $\mathcal{M}_0$  [Eq. (32)] on  $s$  were sufficiently weak that one could ignore the extrapolation off-shell in the pion kinematics. (This could be valid for high energy  $K^+$ , far above threshold and  $K\pi$  resonances—but not at low energies.) Then we write

$$\mathcal{M}_0(s) \approx -8\pi\sqrt{s'}f_0(s') \quad (35)$$

where  $f_0(s')$  is the forward (on-shell)  $K\pi$  c.m. scattering amplitude, evaluated with on-shell kinematics:  $s' = [\omega_\pi(q) + \omega_k(p)]^2 - (\mathbf{q} + \mathbf{p})^2$ . This amplitude may be transformed to the pion rest frame (“lab”—assuming  $\mathbf{p} \parallel \mathbf{q}$ ) by

$$f_{\text{lab}}(\mathbf{p}, \mathbf{q}) = \frac{\sqrt{s'}}{\mathcal{E}_\pi(q)} f_0(s'). \quad (36)$$

Then Eqs. (1) or (9)–(11) may be written

$$F^{\text{MEC}} = 2 \langle \delta n \rangle_A \int d\mathbf{q} \rho_0(\mathbf{q}) f_{\text{lab}}(\mathbf{p}, \mathbf{q}). \quad (37)$$

If we further assume that the  $\mathbf{q}$  dependence of  $f_{\text{lab}}$  is weak enough to allow its removal from the integral, then

$$F^{\text{MEC}} \approx 2 \langle \delta n \rangle_A f_{\text{lab}}(\mathbf{p}, 0), \quad (38)$$

where  $f_{\text{lab}}$  is now evaluated in the target (true laboratory) rest frame. With the optical theorem, we find

$$4\pi \text{Im}(F^{\text{MEC}}) \approx 2 \langle \delta n \rangle p \sigma_{K\pi}(p), \quad (39)$$

which can be evaluated in terms of the experimental total cross section  $\sigma_{K\pi}$ .

This result is similar to that given recently by Akulichev [12], with two differences: (1) A factor of 2 in our result, Eq. (39), comes from including virtual pion pairs [produced or annihilated by the  $K\pi$  interaction; see Fig. 1(b)]. This doubling has also been pointed out [16] for the MEC contribution to the Compton effect. (2) The isoscalar weighting in Eq. (32) is not the simple average given in [12] [Eq. (8)].

More important, the on-shell approximation, particularly applied to  $\text{Im}(F^{\text{MEC}})$  at low energies, is quite inaccurate, since the on-shell kinematics are quite different from the proper off-shell evaluation of  $\mathcal{M}_0(s)$  using Eq. (27). The last columns of Table IV show the results for Eq. (33) calculated with *on-shell* kinematics [but integrated, as in Eqs. (1) or (10)]. This improper assumption will lead to quite different energy dependence and no threshold for  $\text{Im}(F^{\text{MEC}})$ , as would be expected on general kinematic grounds. On the other hand, the on-shell approximation brings about a very small  $\text{Re}(F^{\text{MEC}})$  with an opposite sign for  $600 < p < 900$  MeV/c as compared to that of the off-shell  $K\pi$  amplitude. This very small  $\text{Re}(F^{\text{MEC}})$  is a consequence of cancellation between the linear and resonant terms.

### C. Correction due to consideration of chiral symmetry

In earlier studies of the MEC contributions to pion scattering from nuclei, we have shown that chiral symmetry provides an important constraint on the MEC contributions at low energy [13,14]. This weakly broken symmetry for the pion is particularly useful in selecting diagrams to investigate certain types of meson exchange contributions. For example, in a MEC theory with pion exchange, where the basic interaction is  $\pi$ - $\pi$  scattering, chiral symmetry requires the inclusion of a second process:  $\pi N$  scattering accompanied by a simultaneous exchange of a pion with a second nucleon. The diagrams for these terms are called “pole” and “contact,” respectively [see Figs. 1(a) and 1(b) of Ref. [13]]. However, chiral symmetry also relates the contributions of the two terms [14]. Therefore, the question may arise: What are the consequences of assuming chiral symmetry in the case of  $K^+$ -nucleus scattering?

To investigate the constraint imposed by chiral symmetry in the present context, two considerations are in order. First, the soft kaon theorems (in analogy to the soft pion theorems) appear to apply constraints only to the real parts of the amplitudes. This is because at those specific off-shell points where the soft kaon theorems are defined, the amplitude of Eq. (23) becomes purely real. In fact, the form of the imaginary parts is not derived from the consideration of chiral symmetry but from the uni-

tary condition for  $K\pi$  scattering. Secondly, we do not know whether or how chiral symmetry applies constraints on the resonant terms which are very important in the present work, in particular, to the imaginary part when  $p > 800$  MeV/c. In view of these, we shall assume that chiral symmetry only provides a constraint on the real part of our linear MEC amplitude.

With these assumptions, the chiral-symmetry constraint seems to affect only the first line of Eq. (28a). Using the on-shell constraints Eq. (25), the first term can be shown to be proportional to the isoscalar  $K\pi$  scattering length because of the following:

$$\alpha_0 + 2\beta_0(m_\pi^2 + m_k^2) = -\frac{8\pi}{3}(m_\pi + m_k)(a_1 + 2a_3). \quad (40)$$

(The  $\beta'_0$  term vanishes in the chiral limit  $m_k \rightarrow 0$ .) As shown in Ref. [20], the isoscalar scattering length ( $a_1 + 2a_3$ ) vanishes in the chiral limit, and the first term of Eq. (28a) will vanish accordingly. Therefore, following the argument given in Ref. [14], the second term in Eq. (28a) must be omitted, since in a chiral theory, it will be cancelled by the contact term to have a correct chiral limit. (Again we can show that the remaining terms in linear model vanish in the chiral limit, i.e.,  $m_k \rightarrow 0$ , without further constraint.)

Then, to calculate  $\text{Re}(F^{\text{MEC}})$  in our model with the chiral constraint, we simply omit the term with the integral  $\int d\mathbf{q}(q^2 + m_\pi^2)$  in Eq. (28a). Such a calculation takes into account the corrections due to chiral-symmetry breaking through nonvanishing ( $a_1 + 2a_3$ ) and kaon mass. It is easily seen from the on-shell constraints on the expansion parameters, that the numerical result is exactly the same as that of model (III). The latter has already been discussed in Sec. IV B and the result is shown in Fig. 4. Comparing (III) with (I) (full model), we find that although the chiral-symmetry correction changes the value of  $\text{Re}(F^{\text{MEC}})$  dramatically, it does not change the sign. This tells us that the qualitative conclusion about the MEC contribution to the differential cross section will not be affected by the consideration of the chiral constraint, although its size will be changed (see next section).

To conclude, we would emphasize that the above results should only be considered suggestive, since chiral symmetry for low energy  $K$ 's is not well tested. In fact, chiral symmetry could be severely broken in low energy kaon scattering since its mass is more than three times larger than pion. Further studies are certainly needed in this regard.

## VI. COMPARISON WITH EXPERIMENTS

Recent experiments measure the ratio of total cross section for  $K^+ + {}^{12}\text{C}$  to that of  $K^+ + d$  as a function of  $p$  for a range  $480 < p < 740$  MeV/c [3,4]. An earlier experiment covered the higher-momentum range 700–1000 MeV/c [1]. Data are plotted in Fig. 5 as  $R = \sigma_t({}^{12}\text{C})/6\sigma_t(d)$ , to emphasize the closeness of the ratio to unity. This would be the value in the limiting case that the  $K^+$  scattering on these nuclear targets were given completely by free  $K^+N$  (isoscalar) single scatter-

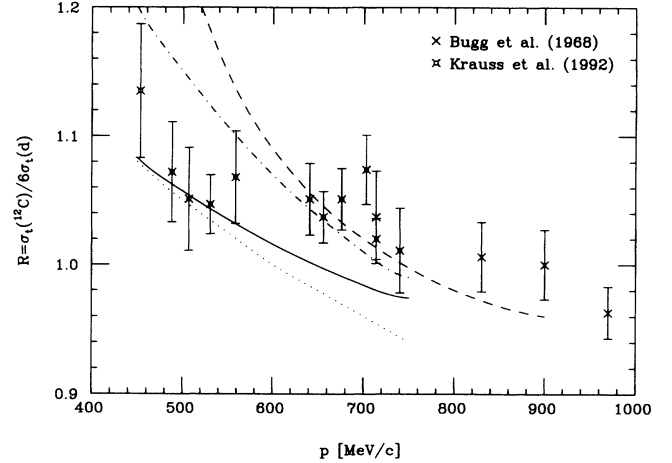


FIG. 5. Comparison of data and our MEC model for the ratio  $R$ : data points from [3,4]; dotted line—optical calculations, from [7]; solid line—this work:  $R_{\text{optical}} + \Delta R$  [Eq. (41)]; “swelling models”: dashed line— [8], dot-dashed line— (10% increase) [7]. (Calculations for  $p < 500$  MeV/c are quoted from [3].)

ing, with no corrections for multiple scattering, including optical potential scattering, meson exchange, or other medium effects.

Microscopic optical model results have been calculated by Siegel, Kaufmann, and Gibbs [7], and are shown by the dotted line of Fig. 5, where values for  $p < 500$  MeV/c are quoted from Ref. [3]. This is actually the upper limit of a range of corrections, and shows that the multiple-scattering corrections tend to underpredict the experimental ratio, by an order of less than or up to 10% for this limit. The range of corrections considered by these authors depresses the curve for the multiple scattering by an almost uniform ratio over the momentum range, giving up to 10% additional reduction.

The general trend of the data is a slower decrease with  $p$  than that of the multiple scattering (upper limit). With the possible exception of the lowest momentum point, the data are in agreement with multiple scattering in the 500–600 MeV/c range. The biggest disagreement is for larger  $p$  where the “shadowing” correction brings the multiple scattering ratio below unity.

The solid line in Fig. 5 shows the effect of adding our MEC correction to the multiple scattering calculation of Ref. [7] (dotted line). This correction is obtained directly from the calculated values of  $\text{Im}[F^{\text{MEC}}(a)]$  of Table III, using the optical theorem to give the ratio

$$\Delta R = \frac{\Delta\sigma^{\text{MEC}}({}^{12}\text{C})}{6\sigma_t(d)} = \frac{4\pi \text{Im}[F^{\text{MEC}}]}{6p\sigma_t(d)} = \frac{\text{Im}[F^{\text{MEC}}]}{12 \text{Im}[F_0^{KN}]}, \quad (41)$$

where, for simplicity, we define  $\text{Im}(F_0^{KN}) = \frac{1}{2}p\sigma_t(d)/4\pi$ . If the  $K^+$  multiple scattering in the deuteron is neglected,  $F_0^{KN}$  then becomes exactly the isoscalar  $K^+N$  scattering amplitude. In Table V, we tabulate values of  $\text{Im}(F_0^{KN})$ ,  $\text{Im}(F^{\text{MEC}})$ , and  $\Delta R$  for the momentum range 400–1200 MeV/c, where  $\text{Im}(F_0^{KN})$  are calculated using

TABLE V. Imaginary forward isoscalar amplitudes (in units of fm) for the  $KN$  scattering ( $F_0^{KN}$ ), and the MEC model ( $F_0^{\text{MEC}}$ ) as well as the ratio  $\Delta R$  defined in Eq. (41).

$p$	$\text{Im}(F_0^{KN})$	$\text{Im}(F_0^{\text{MEC}})$	$\Delta R$
400	0.20	0.0	0.0
500	0.24	0.02	0.007
600	0.32	0.06	0.016
700	0.39	0.11	0.024
800	0.47	0.25	0.044
900	0.56	0.41	0.061
1000	0.68	0.52	0.064
1100	0.81	0.59	0.061
1200	0.92	0.64	0.058

the above definition and the experimental data of Refs. [23,24]. We see that  $\Delta R$  increases with  $p$ , from very small values near 500 MeV/ $c$  ( $\Delta R = 0$  at the threshold of  $\sim 400$  MeV/ $c$ ). The percentage correction is  $\sim 6.4\%$  at 1 GeV/ $c$ . The direction of the change to the multiple-scattering curve brings the total in closer agreement to the trend of the data. The overall scale of  $\Delta R$  is subject to the uncertainties in the pion excess number  $\langle \delta n \rangle_A$ , as discussed in Sec. IV A; we estimated an uncertainty of  $\pm 50\%$  for our values.

An important advantage of our MEC model lies in its evaluation of both the real and imaginary parts of the scattering amplitude. As a result, the effect of the MEC contribution on both total and differential cross sections can be investigated. In the above, we have already learned that  $\text{Im}(F^{\text{MEC}})$  has the same sign as that of the optical model, leading to an improvement over the discrepancy between experimental and optical results. In fact, the real part of the MEC amplitude also has the same sign as the optical model amplitude. This can be seen by comparing the  $\text{Re}(F)$  listed in Table III(a) and Table VI ( $\text{Re}[F_0^{KN}]$  are obtained from data of Ref. [24]). As we mentioned earlier, there exist large uncertainties in the real amplitude as compared with the imaginary part in the present MEC model. Consequently, unlike its contribution to the total cross section, the MEC contribution to the differential cross section depends sensitively on the off-shell extrapolation of the  $K\pi$  amplitude. To show this, we choose two extreme cases [I (full) and III ( $\beta_0 \equiv 0$ ) of Fig. 4] of our MEC model to calculate the percent change of the differential cross section when adding  $F^{\text{MEC}}$  to the optical model amplitude. With the impulse approximation for the latter, this change  $\Delta$  is calculable using

$$\Delta = \frac{|d\sigma(\text{MEC}+KN) - d\sigma(KN)|}{d\sigma(KN)} \quad (42)$$

where

$$d\sigma(KN) = |F_0^{KN}|^2$$

and

$$d\sigma(\text{MEC}+KN) = |F_0^{KN} + F^{\text{MEC}}/A|^2.$$

The numerical results are shown in Table VI. As expect-

ed, the actual changes bear large uncertainties. However, because these uncertainties do not change the sign of the real MEC amplitude, the addition of the MEC effect always gives an increase to the differential cross section, for example, it is at least  $\sim 10\%$  around  $p = 800$  MeV/ $c$ .

The above observations on the real and imaginary amplitudes tell us that the MEC contribution to the  $K^+$ -nucleus scattering will bring a simultaneous increase of both total and differential cross sections. As we noted earlier, the experimental total and differential cross sections are underpredicted by the optical model. The constructive contribution to both cross sections may be a strong indication that the MEC effect does play a role in the  $K^+$ -nucleus scattering. However, to determine completely and quantitatively such a contribution, better models and further studies are needed in order to remove the large uncertainties in the real amplitude.

## VII. CONCLUSIONS

We have calculated the contribution to  $K^+ \text{-}^{12}\text{C}$  amplitudes of  $K^+$  scattering from virtual pions exchanged between nucleon pairs—the meson exchange current. The momentum distribution of virtual pions was adopted from calculations of the *excess pions* in nuclei by several authors [15,19]. Since these results are sensitive to assumptions in the nuclear structure theory from which they were obtained, they should be (and are being) investigated further. This would also be of interest for other experiments which may be sensitive to the pion content of nuclear targets.

We have discussed uncertainties introduced by the assumed form of the off-shell invariant amplitude given in Eq. (23). The two terms were based on an expansion about threshold for  $\mathcal{M}_0^{\text{lin}}$ , and the lowest  $K\pi$  resonance  $K^*(892)$  for  $\mathcal{M}_0^{\text{res}}$ . An improvement of  $\mathcal{M}_0^{\text{lin}}$  which would allow extension of the calculation to higher energies would be to include higher powers in  $s, u, k(s)$ , and  $k(u)$ . In particular, this would introduce  $k^3$  terms in the imaginary part of  $\mathcal{M}_0^{\text{lin}}$ , not given in Eq. (19), and include contributions both from the expansion of  $\sqrt{x}$ , Eq. (24), and from the effective range terms in Eq. (16). The former tends to increase the values of  $\text{Im}(F^{\text{MEC}})$ , the latter is less important. Similarly, adding higher  $K^*$  resonances would be expected to increase  $\text{Im}(F^{\text{MEC}})$  at higher momenta,  $p > 1$  GeV. The effects on  $\text{Re}(F^{\text{MEC}})$  are more complicated. It should be noted that extending  $\mathcal{M}_0^{\text{lin}}$  to higher orders does increase the possibilities for off-shell extrapolation and introduce more freedom in the possible values of the expansion parameters, therefore, even larger uncertainties in the results as compared to the present model. However, constraints due to unitarity limit the form of  $\text{Im}(\mathcal{M}_0^{\text{lin}})$ , making the calculation of  $\text{Im}(F^{\text{MEC}})$  more controlled than that of  $\text{Re}(F^{\text{MEC}})$ , as we have seen earlier.

The question of the importance of other meson exchange processes than those of Fig. 1 has been discussed in Sec. V C. It would be interesting to investigate further the role of (broken) chiral symmetry in such contributions, e.g., along the line of Ref. [14].

We conclude that the MEC contribution to  $K^+ \text{-}^{12}\text{C}$

TABLE VI. The MEC contribution to the differential cross section [see Eq. (42)] showing possible uncertainties because of the off-shell extrapolation: (I) full, (III)  $\beta_0 \equiv 0$ .

$p$ (MeV/c)	$\text{Re}[F_0^{KN}]$ (fm)	$\text{Re}[F^{\text{MEC}}(\text{I})]$ (fm)	$\Delta(\text{I})$ (%)	$\text{Re}[F^{\text{MEC}}(\text{III})]$ (fm)	$\Delta(\text{III})$ (%)
400	-0.31	-1.49	65	-0.35	14
500	-0.30	-1.44	59	-0.30	13
600	-0.28	-1.39	47	-0.25	8
700	-0.25	-1.31	35	-0.17	6
800	-0.22	-1.22	27	-0.08	9
900	-0.20	-1.24	24	-0.10	11
1000	-0.20	-1.31	22	-0.17	12
1100	-0.23	-1.38	21	-0.24	13
1200	-0.31	-1.46	19	-0.32	12

scattering is a real effect, calculable with some uncertainties. The effect adds to that of multiple scattering by a fraction rising to  $\sim 0.06$  for  $\text{Im}(F)$  (or  $\sigma_t$ ) at  $p \leq 1$  GeV/c from a threshold at  $p \sim 400$  MeV/c (see Table V). This energy dependence is a specific feature of a MEC theory, since the threshold enters, through unitarity, from the opening of the  $\pi$ -production channel. We have noted that the near-threshold behavior of the MEC calculation is consistent with the energy dependence of the data (see Fig. 5) in that, when added to the multiple scattering amplitude, the resulting ratio  $R$  has less downward slope, in closer agreement with the trend of the data. By contrast, most “swelling” mechanisms enhance the slope (see Fig. 5).

Our calculations also predict an increase in the differential cross sections at forward angles, but with considerable uncertainty entering with  $\text{Re}(F^{\text{MEC}})$  (see Table VI). The fractional increase is larger than for  $\sigma_t$ , e.g., 0.09–0.27 for  $p = 800$  MeV/c; data at that energy suggest a need for such an increase, but with considerable experimental uncertainty. There is no threshold predicted in this case.

Newer experiments are under way investigating the dependence of  $\sigma_t$  (or  $R$ ) on the target size [5]. Our prediction for the MEC contribution (per nucleon) would give a weak dependence on target  $A$ , essentially scaling with the mean excess pion numbers  $\langle \delta n \rangle_A / A$ , as shown in Eq. (9). According to Ref. [19(a)], this quantity rises

from 0.119 to 0.142 for targets from Al to Pb.

Two remaining questions are not discussed in this paper: How certain is the calculation of the “conventional” multiple-scattering amplitudes for  $K^+ - ^{12}\text{C}$ , and how much room is left for “unconventional” effects, such as nucleon “swelling”? The questions are, of course, related. We have mentioned that Siegel *et al.* [7] estimate a range of uncertainty for their calculation of  $R$  of  $\sim 10\%$ , depending on  $NN$  correlations and  $KN$  form factors, etc. However, Chen and Ernst [11] calculate values of the ratio  $R$  to be even lower (by 5–10%) than those of Ref. [7]; the origin of the difference is not clear. The status of conventional multiple scattering must be clarified in order to understand the size of the discrepancy between the conventional scattering mechanism and the data, as well as any attempt to explain that discrepancy.

#### ACKNOWLEDGMENTS

The authors wish to thank J. Alster, D. Ernst, and R. B. Wiringa for their very helpful correspondence and enlightening discussion, and in particular J. Alster and D. Ernst for providing the most recent data and R. B. Wiringa for sending us his latest results. This research was supported in part by the U.S. Department of Energy under Grant No. DE-FG02-88ER40425 with the University of Rochester. The numerical calculation was carried out using the VAX computer of High Energy Physics group here, to which we are very grateful.

- [1] D. V. Bugg *et al.*, Phys. Rev. **168**, 1466 (1968).
- [2] D. Marlow *et al.*, Phys. Rev. C **25**, 2619 (1982).
- [3] Y. Mardor *et al.*, Phys. Rev. Lett. **65**, 2110 (1990).
- [4] R. A. Krauss *et al.*, Phys. Rev. C **46**, 655 (1992).
- [5] J. Alster, Proceedings of the International Symposium on Hypernuclear and Strange Particle Physics, Shimoda/Japan, 1991 [Nucl. Phys. **A547**, 321c (1992)]; and private communication.
- [6] P. B. Siegel, W. B. Kaufmann, and W. R. Gibbs, Phys. Rev. C **30**, 1256 (1984).
- [7] P. B. Siegel, W. B. Kaufmann, and W. R. Gibbs, Phys. Rev. C **31**, 2184 (1985).
- [8] G. E. Brown, C. B. Dover, P. B. Siegel, and W. Weise, Phys. Rev. Lett. **60**, 2723 (1988).
- [9] W. Weise, Nuovo Cimento **102A**, 265 (1989).
- [10] Ya. A. Berdnikov and A. M. Makhov, Yad. Fiz. **51**, 910

- (1990) [Sov. J. Nucl. Phys. **51**, 579 (1990)].
- [11] C. M. Chen and D. J. Ernst, Phys. Rev. C **45**, 2019 (1992).
- [12] S. V. Akulinichev, Phys. Rev. Lett. **68**, 290 (1992).
- [13] M. F. Jiang and D. S. Koltun, Phys. Rev. C **42**, 2662 (1990).
- [14] D. S. Koltun and M. F. Jiang, Phys. Lett. B **273**, 6 (1991).
- [15] B. L. Friman, V. R. Pandharipande, and R. B. Wiringa, Phys. Rev. Lett. **51**, 763 (1983).
- [16] M. Ericson and M. Rosa-Clot, Phys. Lett. B **188**, 11 (1987).
- [17] (a) H. Jung and G. A. Miller, in *Pion-Nucleus Physics: Future Directions and New Facilities at LAMPF*, Proceedings of the Los Alamos Conference on Pion-Nucleus Physics, edited by R. J. Peterson and D. D. Strottman, AIP Conf. Proc. No. 163 (AIP, New York, 1988); (b) H. Jung and G. A. Miller, Phys. Rev. C **41**, 659 (1990).

- [18] K. Nakano and S. S. M. Wong, *Phys. Lett. B* **257**, 10 (1991).
- [19] (a) E. L. Berger, F. Coester, and R. B. Wiringa, *Phys. Rev. D* **29**, 398 (1984); (b) E. L. Berger and F. Coester, *ibid.* **32**, 1071 (1985).
- [20] B. R. Martin, D. Morgan, and G. Shaw, *Pion-Pion Interaction in Particle Physics* (Academic, New York, 1976), Chaps. 14.1 and 14.3.
- [21] P. Estabrooks *et al.*, *Nucl. Phys.* **B133**, 490 (1978).
- [22] O. Dumbrajs *et al.*, *Nucl. Phys.* **B216**, 277 (1983).
- [23] T. Bowen *et al.*, *Phys. Rev. D* **7**, 22 (1973).
- [24] B. R. Martin, *Nucl. Phys.* **B94**, 413 (1975).